Microstrip Rotman Lens for Mobile Base Station Backbone in Disaster Area Networks

Novia Nurhidayah Prihatiningtyas[a,1], Khoirul Anwar[a,2], Aloysius Adya Pramudita[b,3]

[a] The University Center of Excellence for Advanced Intelligent Communications (AICOMS), Telkom University, Bandung, Indonesia
[b] Internet Of Things Research Center (RC-IoT), Telkom University, Bandung, 40257, Indonesia

Corresponding author: {[1]novianurhidayahp@student,[2]anwarkhoirul@,[3]adyapramudita@}telkomuniversity.ac.id

Abstract— **Mobile Cognitive Radio Base Station (MCRBS) is a technology to recover network communication temporarily in disaster areas. The communications can be built by constructing the backbone network, where it is formed by connecting multiple MCRBSs with point-to-point radio communication link considering the best routing algorithm. The MCRBS antenna system should has an ability on producing the beam into specific direction to establish point-to-point radio communication link. However, there is no capable system to support the MCRBS antenna system for directing the beam. Therefore, it requires a system that can assist in focusing the beam of antenna system for the MCRBSs connectivity. In this paper, we propose Rotman Lens that has beamforming capability to support radio backbone communication for multiple MCRBSs connectivity in post-disaster networks. The Rotman Lens is chosen to generate amplitude and phase shift in performing beamforming technique with simultaneous signal transmissions from MCRBS to others without moving the antenna system. In this research, the Rotman Lens was evaluated through a series of computer simulations and laboratory experiments to investigate the lens performance. The final proposed lens provides the experiment results for all beam ports with an average value both return loss and mutual coupling of less than -15 dB and -20 dB, where the magnitude deviation in average value and the maximum error of phase difference are 1.172 dB and $6.014°$, respectively. The proposed Rotman Lens is also confirmed to be capable of controlling beam with scanning capability of $-27°$, $-14°$, $0°$, $14°$, $27°$ to support wireless communication backbone link among MCRBSs in disaster recovery networks.**

Keywords— **Rotman lens; beamforming network; beamsteering; mobile cognitive radio base station.**

I. INTRODUCTION

Indonesia is the country located on the pacific ring of fire, where there are three major continental plate, i.e., the pacific plate, the Eurasian and the Indo-Australian plates, and Philippines plate [1]. For 90% of natural disaster occurred globally, it is nearly 81% disaster occurring along circum-pacific belt. Therefore, Indonesia becomes one of the countries with high potential for natural disasters, i.e., volcanic eruptions, earthquakes, floods, and tsunamis. The disasters have effected on disturbing cellular communications and caused lost connection in the disaster area. Therefore, the recovery communications are needed to build up the alternative network communications in post-disaster.

Mobile Cognitive Radio Base Station (MCRBS) proposed in [2] is an alternative solution to recovery process during the post-disaster.

Fig. 1 shows the illustration of the post-disaster network recovery scheme, where the MCRBS is used for recurring the cellular network during the post-disaster [3]. The MCRBS should have connectivity between MCRBSs as the backbone link to rebuild network communication. It can be established through point-to-point link via radio communication based on a predefined routing algorithm [4] [5]. The MCRBS requires an antenna as critical system capable of establishing point-to-point link of the radio communication, where the system should be capable of dynamically directing the beam into specific sector by determining MCRBSs at
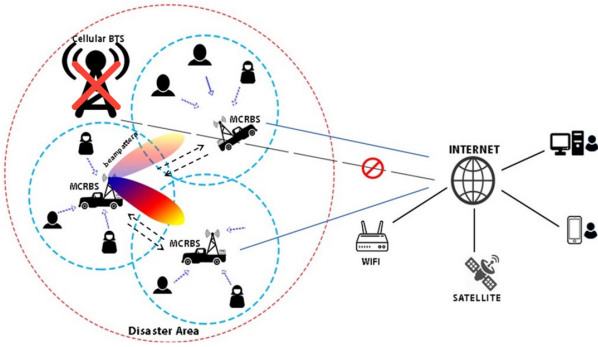
Fig. 1 The illustration of post-disaster network recovery with the help of three MCRBSs

several different positions throughout the disaster area.

The previous studies in [6] and [7], the antenna of MCRBS was designed to serve mobile devices of the second telecommunication generation - the fifth telecommunication generation networks using omnidirectional biconical and directional horn antenna. However, the MCRBS has no system that capable to support antenna system for the connectivity between MCRBS and others by focusing the beam into several sector. Therefore, it requires a system that able to control the beam direction of antenna. The Beamforming network (BFN) is selected for producing feeding phase and amplitude in antenna system to perform beam scanning capability.

The various BFN have developed, i.e., Blass, Butler matrix, Nolen, and Rotman Lens [8]. The Rotman Lens is one of the good candidates of passive beamforming device that providing wide scan angle characteristic, compactness, and easy to fabricate as microstrip model [9] [10]. The Rotman Lens has a capability to simultaneously detect targets in different directions without moving the antenna system [11]. Therefore, in recent years, the Rotman Lens has been implemented in some technology such as for satellite, collision-avoidance radar, and ultra-wideband communication system [8] [12].

In this paper, we propose Rotman Lens to control and steer the beam at specific direction for establishing point-to-point backbone wireless communications. This research contribution is discussing beamsteering by utilizing beamforming network of Rotman Lens with considered as follows:

1) The Rotman Lens propose to support an antenna system for MCRBSs wireless backbone communication at 5.8 GHz.
2) The Rotman Lens beamsteering performance of MCRBS can be directed the beam direction at the five desired angles.
3) Far-field parameters performance of MCRBS radio communications must be established by considering beam direction, covered distance, and horizontal half powerbeamwidth for MCRBSs radio backbone connectivity.

The rest of this paper is organized as follows. The methods and proposed design are explained in Section II. Results and discussion are presented in Section III. Finally, some concluding remarks are presented in Section IV.

II. MATERIALS AND METHODS

This section provides the description of the MCRBS backbone communication system model as shown in Fig. 2. Since the telecommunication infrastructure in the disaster area is damaged, the MCRBS must be recovering the telecommunication infrastructure by considering low power consumption and compact mobility of the MCRBS wireless communication system. By considering those requirements, the MCRBS backbone communications are using Rotman Lens as beamforming network, USRP as the SDR for signal processing, and SPDT switch to select the activated beam port of Rotman Lens. The desired beam pattern is formed in a single narrow beam point by predefined direction of the routing performances. The predefined of routing direction MCRBS with beamforming network is effectively reducing the power consumption of MCRBS due to the MCRBS do not need mechanical azimuth angle position for optimizing radio performances of MCRBS wireless backbone.

A. System Model

To achieve the radio link-budget of MCRBS, the MCRBS antenna with height is approximately 2 meters and the maximum communication link distance (D) of MCRBS is up to 1.5 km. The availability (Av_{path}) backbone link system is also considered by 99.999% for compensate the radio backbone communication link EIRP that impacted to MCRBS communication quality of services. The availability system is calculated by using the fading margin (F_M) value with the land earth factor of ($e = 1$) for the average, flatland, the worst cases of weather factor of ($f = 1$), and considering the center frequency of (f_c) at 5.8 GHz. The fading margin (F_M), following [13] [14], is defined as

$$
\begin{aligned}
F_M &= 30\log D + 10\log(e \times f \times 2.5 \times f_c) - \\
&\quad 10\log Unav_{path} - 60 \\
&= 30\log(1.5) + 10\log(1 \times 1 \times 2.5 \times 5.8) - \\
&\quad 10\log(10^{-5}) - 60 \\
&= 6.89 \text{ dB}, \tag{1}
\end{aligned}
$$

where the unavailability ($Unav_{path}$) is defined as

$$
\begin{aligned}
Av_{path} &= (1 - Unav_{path}) \times 100\% \tag{2} \\
99.999\% &= (1 - Unav_{path}) \times 100\% \tag{3} \\
Unav_{path} &= 0.00001. \tag{4}
\end{aligned}
$$

The fade margin is difference between the received signal level (RSL) and the receiver signal sensitivity (RSS) as the power threshold. The received signal sensitivity (P_{RSSth}) of MCRBS antenna is assumed -110 dBm [15]. Thus, the following relations among F_M, power transmission (P_{Rx}), and P_{RSSth} as power threshold are calculated by

$$
\begin{aligned}
F_M &= P_{Rx} - P_{RSSth} \tag{5} \\
6.89 &= P_{Rx} - (-110) \tag{6} \\
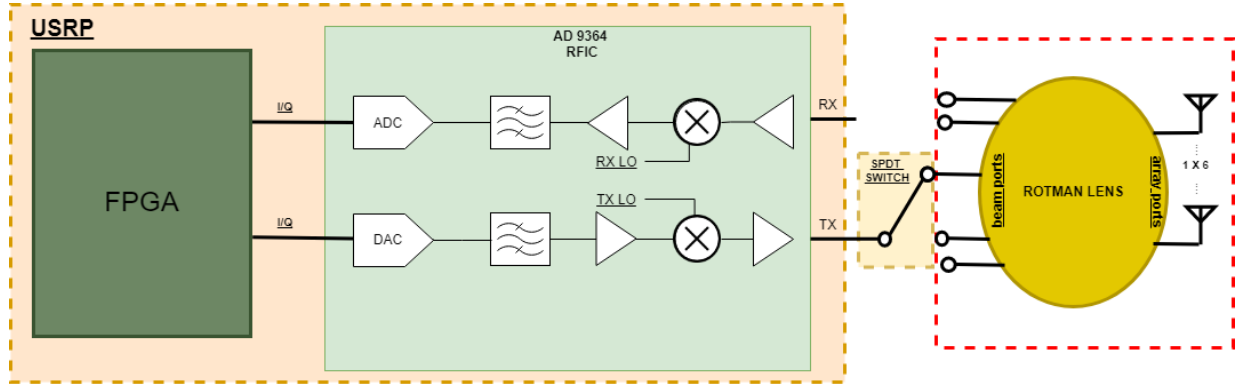P_{Rx} &= -103.10 \text{ dBm}, \tag{7}
\end{aligned}
$$

Fig. 2 Block diagram of MCRBS for backbone communication system

since the transmitter antenna and receiver antenna are in the same ($G_{Rx} = G_{MCRBS}$), the minimum antenna gain can be obtained from the link budget as [15]

$$
\begin{aligned}
P_{Rx} &= P_{MCRBS} - L_{cableTx} + G_{MCRBS} - \quad (8) \\
&\quad L_{RMa-NLOS} + G_{Rx} - L_{cableRx} \\
-103 &= 43 + G_{MCRBS} - 1 - 159.88 + \\
&\quad G_{Rx} - 1 \\
\therefore -103 &= 43 + G_{MCRBS} - 1 - 159.8810 + \quad (9) \\
&\quad G_{MCRBS} - 1 \\
2G_{MCRBS} &= -103 - 43 + 1 + 159.8810 \quad (10) \\
G_{MCRBS} &= 7.95 \text{ dB}, \quad (11)
\end{aligned}
$$

where the defining parameters for the power transmitted (P_{MCRBS}) is 43 dB, loss cable in receiver ($L_{cableTx}$) and transmitter ($L_{cableRx}$) are 1 dB.

The attenuation power transmission between transmitter and receiver in radio communication is considered by the path loss model. The RMa path loss model is chosen as the path loss model, because the model predicts the statistical behavior of received signal strength in rural areas. The model adopts from International Telecommunications Union-Radiocommunications (ITU-R) Sector M.2135. that is defined by [13]

$$
\begin{aligned}
L_{RMa-NLOS} &= 161.04 - 7.1 \log_{10}(W_i) + 7.5 \log_{10}(h) \\
&\quad - (24.37 - 3.7(\frac{h}{h_{BS}})^2) \log_{10}(h_{BS}) + \\
&\quad (43.42 - 3.1 \log_{10}(h_{BS}))(\log_{10}(d_{3D}) \\
&\quad - 3) + 20 \log_{10}(f_c) - (3.2(\log_{10}(11.75 \\
&\quad (h_{UT})))^2 - 4.97),
\end{aligned}
$$

where the street width (W_i) is 50 m; the average building height (h) is 3 m; the base station height (h_{BS}) is 3 m; the mobile (UT) height (h_{UT}) is 3 m; 3D T-R separation distance (d_{3D}) is 1500 m; and the standard deviation (σ_{sf}) is 8 dB. Therefore, the link budget calculation shows that the gain minimum MCRBS antenna is 7.95 dB at both identically transmitter and receiver of MCRBS.

The beamforming capability can be performed by arranging antenna elements. The arranging factors on antenna

TABLE I
PHASE DIFFERENCE FOR EACH SCANNING ANGLES.

Beam Port	5	4	3	2	1
Scanning Angle (θ)	30°	15°	0°	345°	330°
Phase Difference ($\Delta\psi$)	90°	46.58°	0°	−46.58°	−90°

elements are about distance and phase difference between adjacent elements. The phase difference between adjacent elements is influencing delay propagation for each antenna elements. The beamforming studied and performance on array antenna using phase difference concept for each elements is referenced in [16] & [17]. The lens for all beam port to array ports are desired to have perfect linear phase shift for beam scanning. This paper focuses the the adjusted beam direction in -30°, -15°, 0°, $+15^o$, and $+30^o$. The uniform spacing of adjacent elements (d) is applied of $0.5\lambda_0$. In theoretically, the phase shift of lens can be achieved by defining the phase difference between adjacent elements, as follows [16] [17]

$$\Delta\psi = k_0 d \sin(\theta), \quad (12)$$

with the value of k_0 is defined by

$$k_0 = \frac{2\pi}{\lambda_0}, \quad (13)$$

where θ is the desired beam direction, d is the distance between adjacent element, and λ_0 is the wavelength at the design frequency. At a wavelength of λ_0, the phase shift ψ corresponds to time delay that controlling the beam to θ. Table I shows the summary of approximate calculated phase difference by theoretical (12) for switching at desired scanning angle.

B. Microstrip Rotman Lens Design

The Rotman Lens is passive beamforming introduced by Rotman-Tuner in 1963 [18], where the lens equations

are adopted into suitable compact formula by Hansen [12] and Simon [19] then presented based on [20]. Based on the simple ray theory, the equations determine the focal point, the input positions, and array positions. The following equations determine the design of the lens as [18]

$$(\overrightarrow{F_1 P}) + W + \mathrm{N}\sin\alpha = f_2 + W_0, \qquad (14)$$

$$(\overrightarrow{F_2 P}) + W - \mathrm{N}\sin\alpha = f_2 + W_0, \qquad (15)$$

$$(\overrightarrow{F_0 P}) + W = f_1 + W_0, \qquad (16)$$

where the geometry of Rotman Lens comprises a focal arc, paralel plate region, receive contour, and delay lines. The lens contour consists of curve Σ_1 and Σ_2, where the input contour (Σ_1) is defined by the two coordinates (X,Y) and specified relative to O_1 at the central axis of the lens, while then elements on the contour Σ_2 are determined by the single coordinate N and measured relative to the point O_2. The electrical length at the center array contour of (W_0) connects to O_1 and O_2, where O_1 and O_2 are located in the contour Σ_1 and Σ_2, respectively. The coordinate point on array contour of (P) is also connected to coordinate the elements array of (N) by the transmission line of electrical of (W). The lens has three focal points, namely off-axis focal point (F_1) through off-axis focal length of (f_2), off-axis focal point (F_2) through off-axis focal length of (f_3), and on-axis focal point (F_0) through on-axis focal length of (f_1) at the circular beam ports. The path length for focal points of F_1, F_2, and F_0 is defined into $\overrightarrow{F_1 P}$, $\overrightarrow{F_2 P}$, and $\overrightarrow{F_0 P}$, respectively.

The geometry lens also defines f_1 as the lens width at the center, the focal angles (α) as the subtended by upper and lower foci at the center of the element ports curve for the symmetrically lens geometry, the beamsteering angle (θ) as the corresponding to the off-center focal point, location of array ports along array axis of a typical radiating elements (y_3), the coordinate for the array element (N), and the electrical length connecting to the array ports and elements. The parameters are based on the derived equations by Hansen [12], where the design of lens is considered and selected the four basic Rotman Lens parameters (α, β, f_1, and γ). The parameters are convenient to normalize all dimensions by principle of focal length f_1. Furthermore, the focal parameter is defined as ratio of upper and lower focal length f_2 to f_1 as

$$\beta = \frac{f_2}{f_1}. \qquad (17)$$

The array radiates the beam in particular angle from the excited off-axis foci. Thus, the angle ratio of excited off-axis foci and the array are expressed by the expansion factor (γ) where the ratio array beam angle (θ) and lens array angle (α) as

$$\gamma = \frac{\sin\theta}{\sin\alpha}. \qquad (18)$$

In order to realize phase shift, an additional delay line by the normalized length of the cable electrical length (w) is attached to the array elements at $y = y_3$. The equations of
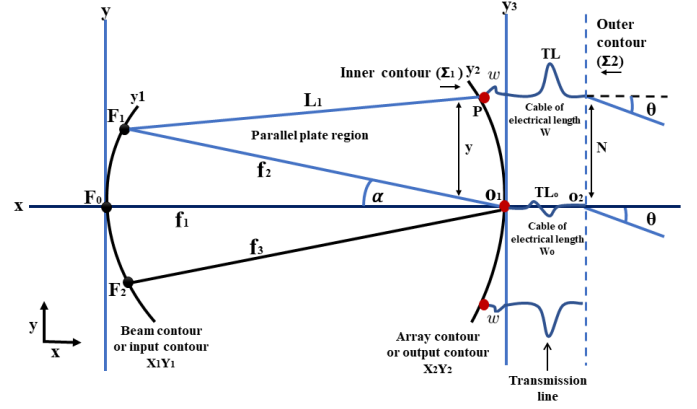

Fig. 3 The geometry of conventional Rotman Lens

quadratic as follows [12] [19]

$$a(\frac{w}{f_1})^2 + b(\frac{w}{f_1}) + c = 0, \qquad (19)$$

where w is normalized relative transmission line length for given parameter of the maximum scanning angle (θ) and focal angles (α). As the solution of quadratic equations, we have a, b, and c defined by

$$a = 1 - \frac{((1-\beta)^2)}{(1-\beta\cos\alpha)^2} - \frac{\zeta^2}{\beta^2}, \qquad (20)$$

$$b = -2 + \frac{2\zeta^2}{\beta} + \frac{2(1-\beta)}{1-\beta\cos\alpha} - \frac{\zeta^2\sin^2\alpha(1-\beta)}{(1-\beta\cos\alpha)^2}, \quad (21)$$

$$c = \zeta^2 + \frac{\zeta^2\sin^2\alpha}{1-\beta\cos\alpha} - \frac{\zeta^4\sin^4\alpha}{4(1-\beta\cos\alpha)^2}, \qquad (22)$$

where ζ is indirect parameter to control the portion of the phase and amplitude error curve of the lens that is expressed as

$$\zeta = \frac{y_3\gamma}{f_1}. \qquad (23)$$

The parameter ζ depends on the position y_3 of any point on the array from the axis toward f_1. The positions of y_3 also effects to the phase. The number of beam port are determined referring for the number of beam direction that needed by the MCRBS system. In this case, the MCRBS requires five directions in beamsteering. Respecting the degree of freedom that required by beamsteering process, the number antenna is six. The array elements spacing in outer contour have selected to be $f_1 = 0.5\ \lambda_0$ for maintaining low mutual coupling between elements. The defining element spacing is to obtain the desired phase difference presented in previous section. The scan angle ($\theta = \pm\ 30°$) is selected to be equal as the focal angle ($\alpha = \pm\ 30°$) in order to keep the geometry of lens compact. The compact lens has trend to minimize spillover loses and make equal the height of curve port that preventing severe asymmetric amplitude reductions and large phase errors [12].

In [12], the α value is used to approximately equalize the curved of the contours and also define the port positions, where the parameter of β also has similar effect to α.

Thus, the pairs of α and β are selected for $\pm 30°$ and 0.90, respectively to produce closely the equal lens shapes and port position. The value of γ is more than 1.0, where the value is chosen considering for the large beam angles implementation, i.e., $30°$.

The taper transition adjusting the flare angles of the ports is crucial design to guarantee smooth energy transition from the input ports through the aperture parallel plate until the receiver ports and radiated elements. An extra transmission line with identical lengths added at the beginning of each taper to prevent the phase error and to assist the implementation of the microstrip-line feed excitation through antenna [21]. Eight dummy ports are symmetrically added on the top and bottom side of the lens for matching load and absorbing the reflected incident signal through the lens. To implement the lens structure design, the dielectric substrate FR-4 epoxy with relative permittivity of ($\epsilon_r = 4.3$) and substrate thickness of ($t = 1.5$ mm) are used, because it is inexpensive and easily found in market. Fig. 4 shows the final design of Rotman Lens.

III. RESULTS AND DISCUSSION

Fig. 5 shows the simulated return loss and measured return loss in Rotman Lens beam ports. The performance on each return loss can be an indicator of the power distribution differences excited into the lens. The lens has a symmetrical design, which causes a symmetrical result. The simulation results have nearly identical value on all symmetrical beam ports, while the measurement show the symmetrical edge beam ports having higher results of return loss than others beam ports. Since the simulated and measured return loss are compared, the average value of return loss in all beam ports of Rotman Lens are less than -15 dB and -18 dB, respectively. Both simulation and measurement results have satisfied the good reflection for less than -10 dB. In terms of

return loss results, the measurement results outperform the simulation results. The measurement performance indicates for SMA connectors in the position off-axis and on-axis beam ports properly installed, whereas excitation power is optimally excited toward Rotman lens connected to antenna.

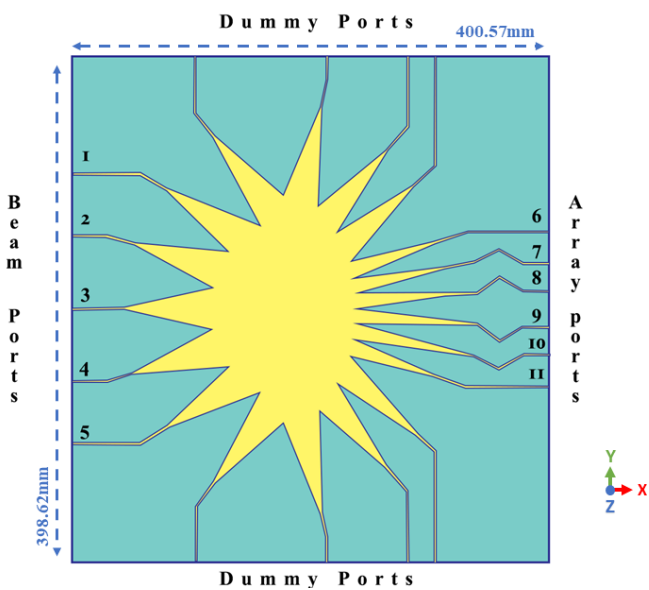The interaction adjacent beam ports on spacing and power losses are observed by coupling performance [22]. The

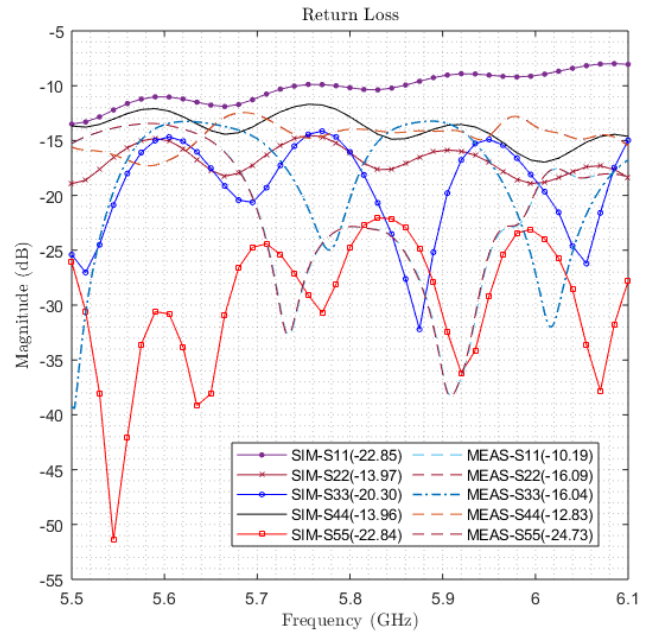Fig. 5 Simulated return loss for five beam ports of the proposed Rotman Lens design
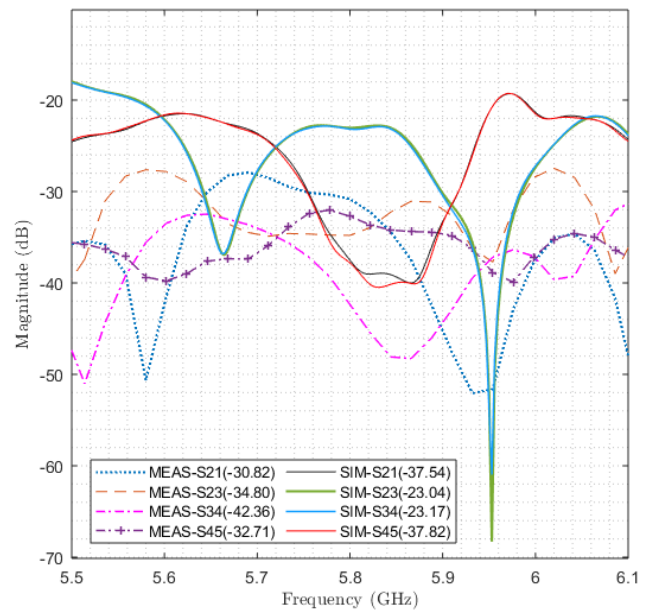
Fig. 4 Final Rotman Lens design

Fig. 6 Simulated coupling between the two adjacent beam ports of the proposed Rotman Lens design

coupling performance can measure aberration parameters which spillover on each beam ports that has an effect on Rotman Lens's efficiency power transmission. Fig. 6 shows the coupling level between the two adjacent beam ports based on simulation and measurement results. According to the simulated results, the coupling level of S23 has symmetrically result with S34 and the coupling level of S21 has symmetrically result with S45. The simulation results have a coupling level which has less than -15 dB on average value, while the measurement has a coupling level which less than -20 dB on average value. The measured results also have outperform than the simulated results, with coupling level has 5 dB higher on average. Therefore, the final results for implementing beam port of lens obtain a good power isolation.

The amplitude is observed to understand the current distribution in the array ports by calculating the standard deviation of amplitude in all array ports. The non-uniform amplitudes that occur through the lens aperture until the array ports referred to amplitude error. In general, the error occurs, each beam ports to array ports has different level of current distribution. In this paper, we investigate from the prospective of power distribution, where both current and power distribution have a linear correlation. We use the standard deviation error to determine and evaluate the error in array ports for each beam port. Fig. 7 illustrates the magnitude error standard deviations across the aperture for all beam ports. The simulation results exhibit the highest magnitude error value in array port 1 and 6, while the measurement results show a range increasing a variation of magnitude error in array ports, with array port 6 and 2 having the highest standard deviation value.

Fig. 7 also shows the comparison between simulation results and measurement results. The measurement results have higher magnitude error than simulation results, which magnitude error for the average values in simulation and measurement are 1.058 dB and 1.172 dB, respectively. However, the magnitude error of measurement are not significantly changed comparing with simulation results. Then,
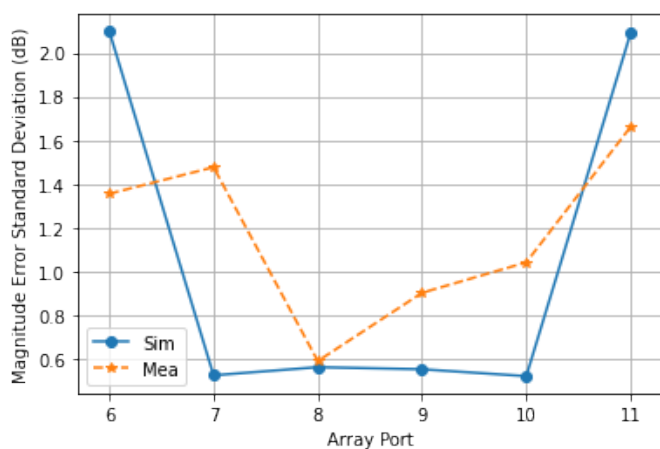
the sidelobe level performance is observed by the effect of magnitude performance. The measured sidelobe level for all beam port that the referenced from edge beam ports has value about less than -11.34 dB, while the simulated sidelobe level about less than -12.34 dB, as shown in Fig. 9. Thus, the magnitude error values do not significantly change the sidelobe level performances.

The controlling phase is important factor for achieving objective beam direction in Rotman Lens beamforming network. Analysing phase shift in Rotman Lens is necessary to evaluate the objective results. The results of phase error are found in both simulation and measurement, where the phase error is defined by a deviation of root mean square error between phase shift from the referenced port (beam port 3) compared with other beam ports.

Fig. 8 presents the phase error for all beam port in simulation results and measurement results. The graph shows the measured phase error for all beam ports are in good agreement with the simulation result. Both simulations and measurement results, the phase error is zero in the center port, while the phase errors increase in the other ports. The phase error is the lowest value in beam ports 3, while the highest phase error is in beam port 1 in and 5. The error phase is occurred, because the unwanted reflection wave from unwanted ports strongly diffracts the transmitted wave to the beam contour area's outer vertices. The unwanted reflected wave may occur in this case due to the efficiency of dummy loads having low manufactured efficiency values.

The phase difference for all beam ports are also calculated by theoretical (12) and investigated by simulation and measurement. We analyze the error of phase difference by comparing the collected data of phase difference from simulations and measurements. Table II shows the comparison results of phase difference for all beam ports, where we found the comparison between simulation result to theoretical results for error of phase difference is less than $1°$. However, the error of phase difference is still tolerated, because the result is still close with the theory of value. The phase differences between measurement results
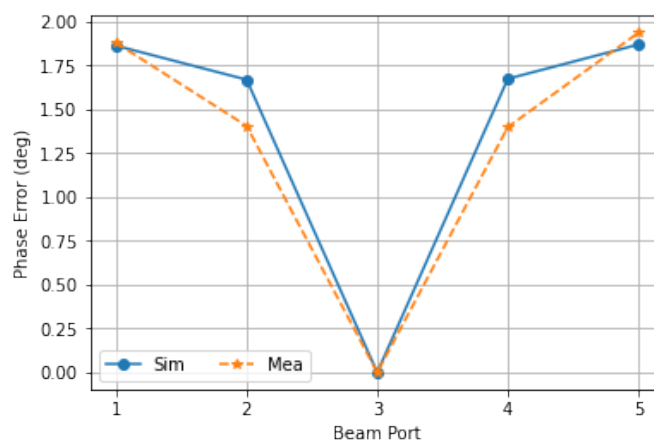

Fig. 7 Magnitude error standard deviation of array port for all beam ports of the proposed Rotman Lens

Fig. 8 Phase error for all beam ports of the proposed Rotman Lens

TABLE II
PHASE DIFFERENCE OF THE PROPOSED ROTMAN LENS.

Beam Port (BP)	Scanning Angel (θ)	Phase Difference ($\Delta\psi$)		
		Theory	Simulation	Measurement
1	$-30°$	$-90°$	$-90.302°$	$-84.486°$
2	$-15°$	$-46.58°$	$-47.382°$	$-45.840°$
3	$0°$	$0°$	$0°$	$0°$
4	$15°$	$46.58°$	$47.388°$	$46.561°$
5	$30°$	$90°$	$90.306°$	$84.292°$

to theoretical results found the greatest error to be in beam port 1 by $5.514°$ and beam port 5 by $5.708°$. Furthermore, the measurement to simulation result has also greatest error about $5.815°$ in beam port 1 and $6.014°$ beam port 5. Thus, as shown in Table II, the performances of phase difference have correlation results with Fig. 8. The phase difference results are influenced by the phase shift, because the phase difference are theoretically correlating with the phase shift distribution in all ports.

The amplitude and phase performance have effects on the sidelobe level and scanning direction, respectively. Thereafter the direction of beam scanning has consequences in the far-field performance for gain and beamwidth. The simulated beam pattern and measured beam pattern are observed by generating the phase performance in Table II and the amplitude performance in Fig. 8. Figs. 9 (a) – 9 (e) illustrate the beam pattern of array factor of designed lens using the method in theory, simulation, and measurement for beam port 1, 2, 3, 4, and 5, respectively. The results show that the beam angle in the proposed lens in simulation gets closer to the angle of theory theoretical very well, where the lens for five beam ports in measurement can steer beam into $-27°$, $-14°$, $0°$, $14°$, $27°$.

Although, the beam directions in simulation results have shifting slight direction unlike the desired scanning angle, however the scanning angle is considered able to satisfy on beamwidth area of beam pattern. While, the measured beam

TABLE III
SIMULATED AND MEASURED BEAM PATTERN RESULTS (SIM. = SIMULATED, MEAS. = MEASURED).

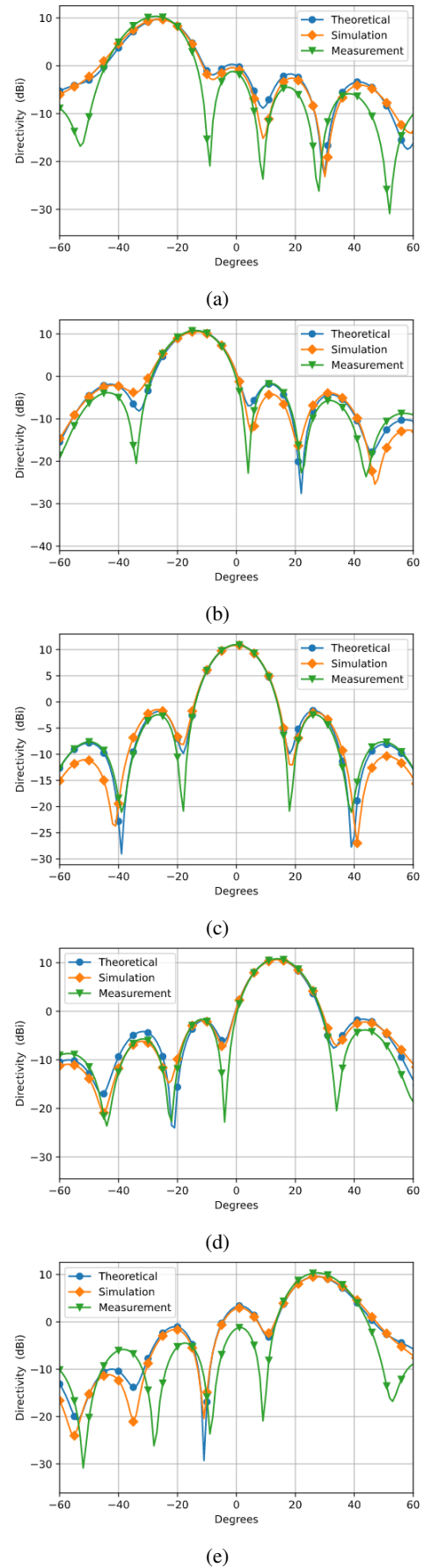| Beam Port	Beam direction		Beamwidth		Directivity	
	Sim.	Meas.	Sim.	Meas.	Sim.	Meas.
1	$-27°$	$27°$	$18.4°$	$19.1°$	13 dB	12.4 dB
2	$-14°$	$-14°$	$17.1°$	$16.9°$	13.2 dB	13.0 dB
3	$0°$	$0°$	$16.2°$	$16.2°$	13.3 dB	13.1 dB
4	$14°$	$14°$	$17.1°$	$16.7°$	13.2 dB	13.0 dB
5	$27°$	$27°$	$18.4°$	$19°$	13.0 dB	12.3 dB

(a)

(b)

(c)

(d)

(e)

Fig. 9 Array factor for five beam ports exited separately. (a) Array factor port number 1. (b) Array factor port number 2. (c) Array factor port number 3. (d) Array factor port number 4. (e) Array factor port number 5

angle is compared simulated beam angle, the results in measurement do not conduct any shifting directions anymore. The measurement very agree with the simulation and not making a problems on constructing the beam scanning. Table III summarizes and compares the far-field performances using different methods. According to the sidelobe level, the center beam port has optimum value, while the more in the edge of position beam ports, the lower value of sidelobe level. It is also applied for the largest beamwidth, the lowest gain. Therefore, the measured results are in good agreement with the simulated results for the performance of beam pattern.

IV. CONCLUSION

This paper has proposed the design of Rotman Lens at 5.8 GHz and provided evaluations via a series of computer simulation followed by real-field measurement. The Rotman Lens design was simplified for the fabrication by using FR-4 substrate. We have simulated and measured Rotman Lens design until the good performances are obtained, in terms of reflection and transmission coefficient. The reflection coefficient of the return loss and coupling performance on an average value showed less than -15 dB and -20 dB, respectively. The transmission coefficient for magnitude performance and phase difference have maximum error at 1.172 dB and $6.014°$, respectively. The proposed Rotman Lens is confirmed to have five beam directions at $-27°$, $-14°$, $0°$, $14°$, $27°$ for support antenna system of wireless backbone communications link among MCRBSs. These results confirm that Rotman Lens are potentially support antenna backbone during link construction in post-disaster by connecting multiple MCRBSs with beamforming capability, especially when the disaster area need to be covered in large area and high mobility of MCRBSs.

REFERENCES

[1] M. R. Amri, G. Yulianti, R. Yunus, A. N. I. Sesa Wiguna, R. E. Randongkir, and R. T. Septian, *Risiko Bencana Indonesia*, 1st ed. Jakarta, Indonesia: Badan Nasional Penanggulanan Bencana, October 2016.

[2] K. Anwar, A. A. Muayyadi, M. A. Murti, E. Kurniawan, R. Mayasari, B. Syihabuddin, N. M. Adriansyah, U. S. R. Nugraha, S. Sumaryo, Y. S. Hidayat, and R. C. Negara, "Recent updates on prevention and recovery networks for indonesia natural disasters based on the intenet-of-things (patriot-net)," *2nd Symposium of Future Telecommunication and Technologies (SOFTT) 2018*, December 2018.

[3] K. Anwar and I. A. Rangkuti, "Header detection of 5G mobile base station for wireless disaster recovery networks," *2nd Symposium of Future Telecommunication and Technologies (SOFTT) 2018*, December 2018.

[4] S. Hartinah, H. Prakoso, and K. Anwar, "Routing of mobile cognitive radio base station for disaster recovery networks," in *2018 International Conference on Electrical Engineering and Informatics (ICELTICs)*, 2018, pp. 1–6.

[5] L. Fauzi, K. Anwar, and Hafidudin, "Experiment of routing for mobile cognitive radio base station (mcrbs)," in *2020 10th Electrical Power, Electronics, Communications, Controls and Informatics Seminar (EECCIS)*, 2020, pp. 307–312.

[6] D. A. Sujiansyah, K. Anwar, and B. Syihabuddin, "Antenna design for multi-generation 2G-5G for rural area wireless commmunication)," *2nd Symposium of Future Telecommunication and Technologies (SOFTT) 2018*, December 2018.

[7] D. A. Sujiansyah, K. Anwar, and A. A. Pramudita, "Biconical antenna for mobile base station for post disaster area wireless communications," in *Symposium on Future Telecommunication Technologies (SOFTT) 2019*, vol. 1, Kuala Lumpur, Malaysia, November 2019, pp. 1–6.

[8] S. Vashist, M. Soni, and P. Singhal, "A review on the development of rotman lens antenna," *Chinese Journal of Engineering*, vol. 2014, pp. 1–9, July 2014.

[9] A. J. Fenn, *Adaptive Antennas and Phased Arrays for Radar and Communications*, 1st ed. Massachusetts, USA: Artech House, 2008.

[10] S. Christie, R. Cahill, N. Mitchell, Y. Munro, and A. Manabe, "Liquid crystal based rotman lens antenna with switchable monopulse patterns," *Microwave and Optical Technology Letters*, vol. 55, pp. 2721–2726, November 2013.

[11] S. Christie, R. Cahill, N. B. Buchanan, V. F. Fusco, N. Mitchell, Y. V. Munro, and G. Maxwell-Cox, "Rotman lens-based retrodirective array," *IEEE Transactions on Antennas and Propagation*, vol. 60, no. 3, pp. 1343–1351, March 2012.

[12] R. C. Hansen, "Design trades for rotman lenses," *IEEE Transactions on Antennas and Propagation*, vol. 39, no. 4, pp. 464–472, April 1991.

[13] G. R. MacCartney and T. S. Rappaport, "Study on 3gpp rural macro-cell path loss models for millimeter wave wireless communications," in *2017 IEEE International Conference on Communications (ICC)*, May 2017, pp. 1–7.

[14] R. L. Freeman, *Telecommunication system engineering*, 4th ed. New York, USA: John Wiley & Sons, Inc., 2004.

[15] G. L. Stüber, *Principles of mobile communication, Fourth Edition*, 4th ed. Atlanta, USA: Springer, 2017.

[16] H. J.Visser, *Array and Phased Array Antenna Basics*, 6th ed. England: John Wiley & Son Ltd, 2005.

[17] R. J. Mailloux, *Phased Array Antenna Handbook*, 3rd ed. London, England: Artech House, 2017.

[18] W. Rotman and R. Turner, "Wide-angle microwave lens for line source applications," *IEEE Transactions on Antennas and Propagation*, vol. 11, no. 6, pp. 623–632, November 1963.

[19] P. Simon, "Analysis and synthesis of rotman lenses," in *22nd AIAA International Communications Satellite Systemns Conference & Exhibit 2004*, vol. 2. Monterey, California: America Institute of Aeronautics and Astronautics,Inc., May 2004.

[20] J. Säily, M. Pokorný, M. Kaunisto, A. Lamminen, J. Aurinsalo, and Z. Raida, "Millimetre-wave beam-switching rotman lens antenna designs on multi-layered lcp substrates," in *2016 10th European Conference on Antennas and Propagation (EuCAP)*, 2016, pp. 1–5.

[21] B.-h. Sun, Q.-y. Liang, and G.-n. Zhou, "Miniaturized rotman lens with applications to wireless communication," *Frontiers of Information & Technology Electronic Engineering*, vol. 21, pp. 144–158, January 2020.

[22] M. Al-Obaidi, E. Mohd, N. Abdullah, S. Dahlan, and J. Ali, "Design and implementation of microstrip rotman lens for ism band applications," in *Bulletin of Electrical Engineering and Informatics*, vol. 8, March 2019, pp. 90–98.